Anion dependence of camel-shape capacitance at the interface between mercury and ionic liquids studied using pendant drop method

Naoya Nishi*, Shunsuke Yasui, Atsunori Hashimoto, and Tetsuo Sakka

Department of Energy and Hydrocarbon Chemistry, Graduate School of Engineering, Kyoto University, Kyoto 615-8510, Japan

*Correspondence should be addressed

Tel: +81-75-383-2491

Email: nishi.naoya.7e@kyoto-u.ac.jp

Abstract

The electrocapillarity and zero-frequency differential capacitance, C_d, have been studied using pendant drop method, at the Hg interface of an ionic liquid (IL), 1-ethyl-3-methylimidazolium bis(trifluoromethanesulfonyl)amide, [C_2mim$^+$][TFSA$^-$], and have been compared with those of [C_2mim$^+$]BF_4^-, an IL with the common cation and a different anion, to focus on the anion dependence of zero-frequency C_d. The Hg interface of [C_2mim$^+$][TFSA$^-$], the IL of the larger anion in the present study, exhibits greater zero-frequency C_d than that of [C_2mim$^+$]BF_4^-, the IL of the smaller anion. This behavior contradicts a simple expectation in which larger ion leads to smaller C_d. This apparent contradiction is explained by proximity of the charged moiety of TFSA$^-$ to the electrode surface compared with that of BF_4^-. The potential dependence of zero-frequency C_d for the two ILs both exhibits one-hump camel shape around the potential of zero charge (E_{pzc}), which has been predicted to be specific behavior of the electrical double layer of ILs by theory and simulation. The humps are located at potentials more negative than E_{pzc}. From a mean-field lattice-gas theory for the EDL in ILs, this negative shift can be interpreted that the charged moiety for C_2mim$^+$ is more easily condensed in the EDL than those for BF_4^- and TFSA$^-$.

Keywords: electric double layer; interfacial structure; interfacial tension; surface tension; electrochemical impedance spectroscopy; electrocapillary curve; slow dynamics; slow relaxation; hysteresis; TFSI

1 Introduction

Ionic liquids (ILs) are liquid salts that are composed of cations and anions and the possible electrochemical applications of ILs have recently accelerated studies on the structure of the electrochemical interface of ILs.[1–4] The differential capacitance (C_d) reflects the interfacial structure and its potential dependence, i.e., the behavior of ions in the electrical double layer (EDL). Since ILs are entirely composed of ions without neutral solvent molecules, the potential dependence of C_d has been predicted[3,5,6] to be different from that of the Gouy-Chapman-Stern (GCS) model,[7–9] which has successfully modeled the EDL for dilute electrolyte solutions where neutral solvent molecules are the major components. The mean-field lattice-gas model for the EDL in ILs proposed by Kornyshev[5] illustrates the peculiar camel-shape potential dependence of C_d: either of one-hump or two-hump shape around the potential of zero charge (E_{pzc}) depending on the size of charged and neutral moieties of IL ions,[10–13] in contrast to the U shape behavior for the GCS model. The one-hump camel shape is for ILs composed of small ions and can be explained by excluded volume not only between electrode and ions, but also between neighboring ions in the EDL, the latter of which was not taken into account in the GCS model. The two-hump camel shape is for ILs with relatively large ions having neutral moiety and is similar to the one-hump shape except around E_{pzc} where the potential dependence of C_d returns to the GCS behavior, showing negative curvature. This is due to the neutral moiety in IL ions that can play a role as "latent void"[10,11] to be replaced with charged moiety in IL ions at the first ionic layer when the interface becomes charged from E_{pzc}.

Experimentally, C_d can be measured by using electrochemical impedance spectroscopy (EIS) at a frequency or a range of frequency and by adopting one of probable equivalent circuit models. The EIS C_d for the electrochemical interface of ILs has been intensively reported.[14–24] However, the EIS C_d is known to have strong frequency dependence[25–32] and also hysteresis effect,[25,33–35] both of which seem to result from the structural ordering of IL interface[36–42] and the ultraslow dynamics[43–50] of such ordered structure. This makes it difficult to compare the EIS C_d with C_d from theory and simulation, latter of which is C_d in equilibrium, i.e., zero-frequency C_d. This problem has been pointed out by Fedorov and Kornyshev in their recent review[3] as "*The fact that impedance measurements cannot reliably assess equilibrium characteristics is not a problem of the EDL theory that operates with equilibrium properties, but rather a problem of experimental techniques available these days.*" Therefore, the experimental method that can evaluate zero-frequency C_d would be desirable to compare experimental and theoretical zero-frequency C_d, extract the characteristics of the EDL in ILs from the comparison, and furthermore provide feedbacks for the improvement of the theory of the EDL in ILs.

Recently, we experimentally obtained zero-frequency C_d from the thermodynamic analysis of the electrocapillarity (interfacial tension as a function of electrode potential) at the IL|Hg interface measured using the pendant drop method.[51] Since the pendant drop method is a static method, the measurements are not affected by the ultraslow dynamics of the interfacial structure of ILs, enabling us to experimentally evaluate zero-

frequency C_d and to directly compare it with the prediction by theory and simulation. It should be noted that similar methods to measure electrocapillarity such as drop time method[15,52–57] and drop weight method[58] previously reported for IL|Hg interface, are dynamic ones, which cannot escape from the slow dynamics problem. The potential dependence of zero-frequency C_d obtained using the pendant drop method exhibited remarkable dependence on alkyl chain length of IL cations. $[C_2mim^+]BF_4^-$, IL of cation having short alkyl chain, showed the one-hump potential dependence, whereas $[C_8mim^+]BF_4^-$ with long alkyl chain, i.e., large neutral moiety, showed two-hump camel shape ($C_n mim^+$: 1-alkyl-3-methylimidazolium). These findings experimentally proved the validity of the prediction by theory and simulation.[3,5,10]

In the present study, we further explore the dependence of zero-frequency C_d on ionic species of ILs, by studying the electrocapillarity and the zero-frequency C_d at the Hg interface of $[C_2mim^+][TFSA^-]$ ($TFSA^-$; bis(trifluoromethanesulfonyl)amide) and by comparing them with those of $[C_2mim^+]BF_4^-$ previously studied by us.[51] Although we previously used the mean-field lattice-gas theory for ILs composed of same size ions for analysis, in the present study we used an extended version of the theory recently proposed by Han and coworkers[59] where the size of IL ions can be different. The theory enables us to discuss the difference in the behavior of cation and anion in the EDL from the zero-frequency C_d data. $TFSA^-$ is one of the most frequently used IL anions and the behavior of $[C_2mim^+][TFSA^-]$ at the electrode interface has been studied by experiment[15,37,41,55,57,58,60,61] and simulation.[62–66] $TFSA^-$ has three-time larger volume than BF_4^- (Table 1), and has asymmetric structure and localized charge distribution compared with BF_4^-. We will discuss the effect of these difference of the molecular structure on the macroscopic zero-frequency C_d behavior.

2 Experimental

For the preparation of $[C_2mim^+][TFSA^-]$, equimolar amount of synthesized[51] $[C_2mim^+]Br^-$ and purchased $Li^+[TFSA^-]$ (Central Glass Co.) were dissolved in water and $[C_2mim^+][TFSA^-]$ in the aqueous solution was extracted to dichloromethane. Dry Na_2SO_4 and $MgSO_4$ solids were added to the dichloromethane solution to remove water and the solids were then filtered off. $[C_2mim^+][TFSA^-]$ dissolved in dichloromethane was purified by column chromatography with activated carbon and silica gel as the stationary phase.[43,67] Dichloromethane was removed using an evaporator and a rotary oil pump, and $[C_2mim^+][TFSA^-]$ was obtained as colorless liquid.

The details of the pendant drop method have been reported previously.[51] A pendant drop of Hg hanging from a glass tube immersed in $[C_2mim^+][TFSA^-]$ was illuminated and the shape of the Hg drop was imaged. The outline of the drop was fitted with the theoretical curve of Bashforth-Adams equation. In the fitting the densities, ρ, of the two liquids were fixed and the interfacial tension, σ, was evaluated from one of the variable parameters.[51] The ρ value for $[C_2mim^+][TFSA^-]$ was measured to be 1.520 g cm^{-3} at 25.0 °C by using a density meter (DA-505, KEM), which agrees with literature values.[68,69] The ρ value for Hg was adopted to be 13.5336 g cm^{-3} at 25.0 °C from literature.[70] The potential at the IL|Hg interface was controlled

with a three-electrode electrochemical system. A Ag wire coated with AgCl was directly immersed in the IL as a quasi-reference electrode (QRE), and a Pt coiled wire as a counter electrode (CE). The potential of the Hg working electrode (WE) with respect to the Ag/AgCl QRE, denoted as E, was controlled using a PC-controlled potentiostat (HA1010mM1A, Hokuto Denko). At each potential, measurements were continued for sufficiently long time, typically more than 5 min to equilibrate the interfacial structure at the IL|Hg interface.[51] The σ value that became independent of time was adopted as σ in equilibrium at the potential. Measurements were performed at 25.0±0.1 °C. The surface charge density on Hg, q_{M}, was evaluated from the numerical differentiation of the E dependence of σ in the same manner as previously reported.[51] Similarly, the zero-frequency C_{d} was evaluated from the numerical differentiation of the potential dependence of q_{M} with respect to E.

To compare with the zero-frequency C_{d}, the EIS C_{d} was also measured. A hanging mercury drop electrode (WK2, Institute of Physical Chemistry Polish Academy of Sciences) was used as WE. The surface area of Hg, A, was 0.024 cm^2. QRE and CE are the same as those in the pendant drop method. The EIS measurements were performed with a PC-controlled potentiostat (CompactStat, Ivium Technologies) with the ac potential amplitude of 10 mV and the frequency range from 10 to 1000 Hz. For the analysis of impedance spectra we used equivalent circuit composed of constant phase element (CPE), whose impedance is $\frac{1}{(i\omega)^p T}$ where ω is angular frequency, in series with a solution resistance. When needed, an electron-transfer resistance was added in parallel with CPE. The EIS C_{d} was evaluated as

$$C_{\mathrm{d}} = \frac{T\omega^{p-1}}{A} \tag{1}$$

As shown in Eq.1, C_{d} of CPE depends on the frequency. As a representative data we chose C_{d} at 100 Hz, which corresponds to the midpoint of the measurement frequency range in logarithmic scale. Before measurements at each dc potential, we applied the dc potential for 60-100 s to minimize the effect of the ultraslow dynamics of EDL.

3 Results and Discussion

The electrocapillary curve at the $[C_2mim^+][TFSA^-]$|Hg interface is shown in Fig.1 as solid circles. The shape of σ as a function of E is parabolic and the potential at the apex of the parabola around −0.4 V, is the potential of zero charge, E_{pzc}, where the interface is not charged ($q_{\mathrm{M}} = 0$). In Fig.1 also shown is the electrocapillary curve at the $[C_2mim^+]BF_4^-$|Hg interface (solid squares) from our previous study.[51] The σ value for $[C_2mim^+][TFSA^-]$ at E_{pzc}, 355 mN m^{-1}, which is 34 mN m^{-1} less than that for $[C_2mim^+]BF_4^-$. The interfacial tensions of the free surface (IL|air interface) of the two ILs also have similar tendency: 35.63 mN m^{-1} for $[C_2mim^+][TFSA^-]$ (measured by us) vs 54 mN m^{-1} for $[C_2mim^+]BF_4^-$.[71] This tendency seems to be mainly due to the larger size of $TFSA^-$ compared with BF_4^- (Table 1), leading to smaller surface ionic density and therefore smaller electrostatic attraction energy between neighboring cations and anions. This idea

is supported by previous theoretical consideration of the surface tension of various high-temperature molten salts.[72] One can also see in Fig.1 that the curvature for $[C_2mim^+][TFSA^-]$ is larger than that for $[C_2mim^+]BF_4^-$, which means that the zero-frequency C_d for $[C_2mim^+][TFSA^-]$ is larger than that for $[C_2mim^+]BF_4^-$ since $C_d = -\left(\frac{\partial^2\sigma}{\partial E^2}\right)$. This tendency is counterintuitive, when we recall the Helmholtz model,[73] $C_d = \frac{\epsilon}{r}$, where ions with greater radius, r, leads to smaller C_d, taking into account ϵ, static permittivity, of the two ILs are similar to each other.[74] The negative charge of $TFSA^-$ is relatively localized on N and O atoms[75] and $TFSA^-$ at the electrode interface can have an orientation in which the negative charge sites are close to the electrode surface.[76] In such orientation, r should be small compared with the value simply expected from the ionic volume (Table 1). In contrast, BF_4^- is symmetric and such orientation effect cannot be expected. This idea of charge distribution within anion explains the contradiction, greater C_d for larger $TFSA^-$ anion, observed above.

The q_M values were evaluated by the the numerical differentiation of σ with respect to E. Fig. 2 shows the q_M values as a function of E at the $[C_2mim^+][TFSA^-]$|Hg interface (solid circles) along with those at $[C_2mim^+]BF_4^-$|Hg interface (solid squares).[51] In addition to general trend that the q_M values increase at more positive potentials, one can find a non-monotonic increase in q_M. Such a non-monotonic potential dependence of q_M reflects the potential dependence of the zero-frequency C_d, since $C_d = \left(\frac{\partial q_M}{\partial E}\right)$. The slope of the plots for $[C_2mim^+][TFSA^-]$ is greater than that for $[C_2mim^+]BF_4^-$ as a whole, indicating again that zero-frequency C_d is greater for $[C_2mim^+][TFSA^-]$. Inset in Fig.2 is a magnified figure of the q_M vs. E plots around $q_M = 0$ to evaluate E_{pzc} by finding E at $q_M = 0$. By using the local quadratic approximation around $q_M = 0$, E_{pzc} was evaluated to be -0.373 ± 0.002 V for the $[C_2mim^+][TFSA^-]$|Hg interface, while E_{pzc} for the $[C_2mim^+]BF_4^-$|Hg interface was -0.424 ± 0.012 V. The E_{pzc} data will play a key role as "reference" potential when we discuss the potential dependence of the zero-frequency C_d below.

The zero-frequency C_d values were evaluated by the numerical differentiation of q_M. Fig.3 shows zero-frequency C_d for the $[C_2mim^+][TFSA^-]$|Hg interface (solid circles in Fig.3a) and $[C_2mim^+]BF_4^-$|Hg interface (solid squares in Fig.3b)[51] with the vertical dotted lines at E_{pzc}. One can notice several features from the data. Firstly, for both the ILs, the zero-frequency C_d exhibits one-hump camel-shape potential dependence that has a local maximum near E_{pzc}. Such a local maximum around E_{pzc} is opposite to the global minimum at E_{pzc} predicted from GCS model but agrees with the prediction by recent theories for the EDL of ILs as explained in Introduction.[3,5,6] Secondly, the local maximum of the zero-frequency C_d is more negative than E_{pzc} for both the ILs. The shift is the symptom of ion-size asymmetry, as suggested from theory[5,59,77–79] and simulation;[78,80–82] i.e., when the anion is larger than cation, the local maximum shifts negatively. If we simply refer to ionic volume (Table 1) this negative shift agrees for the $[C_2mim^+][TFSA^-]$ case but disagrees for the $[C_2mim^+]BF_4^-$ case. This point will be discussed below with fitting results. Thirdly, the local maximum value of the zero-frequency C_d for $[C_2mim^+][TFSA^-]$ is higher than $[C_2mim^+]BF_4^-$, as was seen in the curvature of the electrocapillarity in Fig.1 and the slope of the q_M plots in Fig.2. Fourthly, far from the local maximum, i.e., at $E \gg E_{pzc}$, the zero-frequency C_d increases. This "wing" phenomenon was also observed at the aque-

ous solution|Hg interface[83] and in our previous study at the IL|Hg interface.[51] For the IL|Hg interface, the results of in-situ spectroscopic ellipsometry suggest that this increase in the zero-frequency C_d is likely due to densification of the ionic layers in the EDL.[51,84]

The EIS C_d is also shown in Fig.3 as open symbols for comparison. The EIS C_d increases with increase in the potential and this tendency agrees with previous studies,[15,55,57,60] although the EIS C_d values are different possibly due to frequency dependence or hysteresis effect, inherent to the EDL in ILs as described in Introduction. One can see smaller EIS C_d compared with zero-frequency C_d for both the two ILs. The smaller EIS C_d indicates that the EDL of ILs cannot fully be charged during a.c. potential perturbation and that slow components of C_d cannot be captured by EIS. The potential dependence of the EIS C_d is more gradual than that of zero-frequency C_d and does not have one-hump shape around E_{pzc}. This gradual behavior is likely to be caused by slow exchange of ions in the EDL, suggested by studies using surface plasmon resonance[47] and surface-enhanced IR absorption spectroscopy[85] at IL|Au interface. The wing at $E \gg E_{pzc}$ is not observed in the EIS C_d as well. The densification of the ionic layers in the EDL is also likely to decelerate ionic rearrangement, resulting in a large discrepancy between the EIS C_d and the zero-frequency C_d.

To quantitatively analyze the potential dependence of zero-frequency C_d, we used an analytical equation from recent mean-field lattice-gas theory for ILs composed of size-asymmetric ions:[59]

$$\begin{aligned}\frac{C_d}{C_{d,0}} = &\left| -\exp(-u_0) + \exp(u_0)\left[\frac{\xi\exp(u_0)+\eta}{\xi+\eta}\right]^{\frac{1}{\xi}-1}\right| \\ &\times\left[\sqrt{2\gamma_C}\left\{\exp(-u_0) + (\xi+\eta)\left[\frac{\xi\exp(u_0)+\eta}{\xi+\eta}\right]^{\frac{1}{\xi}}\right\}\right. \\ &\left.\times\sqrt{\ln\left\{\exp(-u_0) + (\xi+\eta)\left[\frac{\xi\exp(u_0)+\eta}{\xi+\eta}\right]^{\frac{1}{\xi}}\right\} + \ln\left(\frac{\gamma_C}{2}\right)}\right]^{-1}\end{aligned} \tag{2}$$

with

$$\xi = \frac{\gamma_A}{\gamma_C}$$
$$\eta = \frac{2}{\gamma_C} - 1 - \xi$$

where $C_d/C_{d,0}$ is the normalized zero-frequency C_d and $u_0 = \frac{F(E-E_{pzc})}{RT}$ is the normalized potential with the Faraday constant F, the gas constant R, and the absolute temperature T. Here the compacity, γ_i, of the ion i (i=C for cation and A for anion) is

$$\gamma_i = \frac{c_{bulk}}{c_{i,max}} \tag{3}$$

where c_{bulk} is the concentration of ions in bulk (note that this is twice the concentration of the cation or the anion in bulk) and $c_{i,max}$ is the maximum local possible concentration of the charged moiety of the ion i. ILs having large neutral moiety such as $[C_8mim^+][BF_4^-]$ have small compacity, which leads to two-hump potential dependence of zero-frequency C_d.[51] On the other hand, one-hump behavior observed in the present study implies that γ_i is relatively large for the ions in the two ILs.

The Eq.2 from the mean-field lattice-gas theory include steric effect between ions but does not include another important feature of the EDL in ILs: overscreening effect.[5] Models taking into account the overscreening effect have been proposed[86] and intensively studied.[87–90] Very recently, a perturbation-theory approach to develop an extended version of the mean-field lattice-gas theory that takes into account short-range correlation between ions has also been presented.[91] The mean-field theory without the overscreening effect has been found to overestimate C_d.[86] However, the "overestimation coefficient", the extent of the overestimation, is almost constant within the potential range not far from E_{pzc}, up to around a few hundred mV.[86] With $C_{d,0}$ as a scaling parameter, we still can discuss the potential dependence of our experimental zero-frequency C_d by using Eq.2.

We fitted Eq.2 to the experimental data for the potential dependence of zero-frequency C_d. We limited the fitting region around E_{pzc} because at potentials far from E_{pzc} the wing effect (rise of zero-frequency C_d) is observed and the cause, which is the densification of ionic layers, is not taken into account in the theory. The fitting parameters are γ_C, γ_A, and $C_{d,0}$, with the fixed parameter of E_{pzc} obtained in Fig.2. The fitted curves are shown in Fig.3 as dashed lines and the fitted parameters are listed in Table 2. The $C_{d,0}$ value for $[C_2mim^+][TFSA^-]$, 57 μF cm^{-2}, is 1.7 times higher than that for $[C_2mim^+]BF_4^-$, 34 μF cm^{-2}, again, which can be explained by the asymmetry of the $TFSA^-$ shape. The γ_i values for $[C_2mim^+][TFSA^-]$ are similar to or slightly smaller than those for $[C_2mim^+]BF_4^-$, indicating that "compacity" of ions in these ILs is similar. Although $TFSA^-$ has three-time larger volume than BF_4^-, the charged moiety of $TFSA^-$ cannot be condensed in the EDL significantly more than BF_4^-. In other words, the neutral moiety of $TFSA^-$, if exists, cannot play a role as "latent void" in the EDL. The γ_C value is lower than γ_A for both the ILs, which means smaller size for the charged moiety of C_2mim^+ than $TFSA^-$ and BF_4^-. Quantitatively, the size ratio of the charged moieties between cation and anion is obtained from $\xi = \gamma_A/\gamma_C$ and is listed in Table 2. To compare with ξ, we also estimated the ionic volume, V_i (the sum of the charged and neutral moieties) by using quantum chemical calculation. The ionic volumes for ions are listed in Table 1 and the ratio, V_A/V_C, is in Table 2. The V_i value for C_2mim^+ is smaller than that for $TFSA^-$, which accords with $\xi = 2.1 > 1$ for $[C_2mim^+][TFSA^-]$. On the other hand, it is larger than that for BF_4^-, opposite tendency to the size of the charged moiety for the two ions. This might indicate that C_2mim^+ has relatively big neutral moiety and small charged moiety. However, such small volume of the charged moiety is unreasonable because the positive charge of C_2mim^+ is delocalized over the imidazolium ring, major part of C_2mim^+ structure. Factors missed in the mean-field lattice-gas model include orientation of IL ions at the interface. Several experimental[85,92,93] and simulation[94–97] studies have revealed that C_nmim^+ cations in ILs at the electrode interface have preferential orientation which depends on the potential and the IL kinds. The orientation and its potential dependence are expected to affect the zero-frequency C_d behavior, although it is still unclear how they affect, due to the lack of available theory. To clarify the effect of the ionic orientation on zero-frequency C_d behavior, MD simulation for the EDL at the IL|Hg interface would be desirable as has been performed for the EDL at aqueous solution|Hg interface.[98]

4 Conclusions

We evaluated and compared the zero-frequency C_d and its potential dependence for the EDL at the Hg interfaces of two ILs, $[C_2mim^+][TFSA^-]$ and $[C_2mim^+]BF_4^-$ by using pendant drop method. This method enables us to overcome strong frequency dependence and hysteresis effect of C_d at the interface of ILs and therefore to directly compare the C_d behaviors of the two ILs each other and also compare them with the recently proposed EDL theory for ILs. The usage of Hg, a liquid metal, is another advantage since otherwise we need to significantly consider crystal planes of solid metal surface and long-term contamination hysteresis, although we may keep in mind possible chemical interactions between Hg surface and IL ions. The zero-frequency C_d for $[C_2mim^+][TFSA^-]$ is distinctly higher than that for $[C_2mim^+]BF_4^-$ despite larger $TFSA^-$ size than BF_4^-. This counterintuitive result is explained by the localized negative charge of $TFSA^-$, leading to the formation of thinner EDL than BF_4^-. Comparison of the zero-frequency C_d with the mean-field lattice-gas theory suggests that C_2mim^+ is more easily condensed in the EDL than either of $TFSA^-$ or BF_4^-. This suggestion cannot be rationalized only by the volume of the charged and neutral moieties of the ions, implying that the orientation of ions is one of the essential factors to determine the zero-frequency C_d behavior.

Acknowledgements

This work was partly supported by a Grant-in-Aid for Scientific Research (Nos. 26410149, 26248004,16H04216).

Table 1: Volume of ions by quantum chemical calculation in the level of B3LYP/6-311++G**.

Ion	V_i (cm^3 mol^{-1})
$TFSA^-$	123[a], 128[b]
BF_4^-	45
C_2mim^+	88

[a] C_1 conformer. [b] C_2 conformer.

Table 2: Parameters for the fitting in Fig.3 using Eq.2.

IL	C_0 (μF cm^{-2})	γ_C	γ_A	E_{pzc} (V)	$\xi(=\gamma_A/\gamma_C)$	V_A/V_C [a]
$[C_2mim^+][TFSA^-]$	57±3	0.23 ±0.03	0.48 ±0.06	−0.373 [b]	2.1±0.2	1.4
$[C_2mim^+][BF_4^-]$	34±3	0.30 ±0.07	0.50 ±0.14	−0.424 [b]	1.7±0.4	0.51

[a] Calculated from V_i in Table 1. [b] Fixed to the value evaluated from Fig.2.

References

(1) M. Armand, F. Endres, D. R. Macfarlane, H. Ohno, and B. Scrosati, *Nat. Mater.*, 2009, **8**, 621–629.

(2) ed. H. Ohno, *Electrochemical Aspects of Ionic Liquids*, Wiley, Hoboken, 2nd ed., 2011.

(3) M. V. Fedorov and A. A. Kornyshev, *Chem. Rev.*, 2014, **114**, 2978–3036.

(4) R. Hayes, G. G. Warr, and R. Atkin, *Chem. Rev.*, 2015, **115**, 6357–6426.

(5) A. A. Kornyshev, *J. Phys. Chem. B*, 2007, **111**, 5545–5557.

(6) K. B. Oldham, *J. Electroanal. Chem.*, 2008, **613**, 131–138.

(7) L. G. Gouy, *J. Phys.*, 1910, **9**, 457–468.

(8) D. L. Chapman, *Phil. Mag.*, 1913, **25**, 475–481.

(9) O. Stern, *Z. Elektrochem.*, 1924, **30**, 508–516.

(10) M. V. Fedorov, N. Georgi, and A. A. Kornyshev, *Electrochem. Commun.*, 2010, **12**, 296–299.

(11) N. Georgi, A. A. Kornyshev, and M. V. Fedorov, *J. Electroanal. Chem.*, 2010, **649**, 261–267.

(12) M. Trulsson, J. Algotsson, J. Forsman, and C. E. Woodward, *J. Phys. Chem. Lett.*, 2010, **1**, 1191–1195.

(13) W. Silvestre-Alcantara, M. Kaja, D. Henderson, S. Lamperski, and L. B. Bhuiyan, *Mol. Phys.*, 2016, **114**, 53–60.

(14) R. J. Gale and R. A. Osteryoung, *Electrochim. Acta*, 1980, **25**, 1527–1529.

(15) C. Nanjundiah, S. F. McDevitt, and V. R. Koch, *J. Electrochem. Soc.*, 1997, **144**, 3392–3397.

(16) M. T. Alam, M. M. Islam, T. Okajima, and T. Ohsaka, *Electrochem. Commun.*, 2007, **9**, 2370–2374.

(17) M. M. Islam, M. T. Alam, and T. Ohsaka, *J. Phys. Chem. C*, 2008, **112**, 16568–16574.

(18) M. M. Islam, M. T. Alam, T. Okajima, and T. Ohsaka, *J. Phys. Chem. C*, 2009, **113**, 3386–3389.

(19) Y. Z. Su, Y. C. Fu, J. W. Yan, Z. B. Chen, and B. W. Mao, *Angew. Chem.-Int. Edit.*, 2009, **48**, 5148–5151.

(20) B. Bozzini, A. Bund, B. Busson, C. Humbert, A. Ispas, C. Mele, and A. Tadjeddine, *Electrochem. Commun.*, 2010, **12**, 56–60.

(21) J. P. Zheng, P. C. Goonetilleke, C. M. Pettit, and D. Roy, *Talanta*, 2010, **81**, 1045–1055.

(22) L. Siinor, K. Lust, and E. Lust, *J. Electrochem. Soc.*, 2010, **157**, F83–F87.

(23) T. F. Esterle, D. Sun, M. R. Roberts, P. N. Bartlett, and J. R. Owen, *Phys. Chem. Chem. Phys.*, 2012, **14**, 3872–3881.

(24) Q. Zhang, Y. Han, Y. Wang, S. Ye, and T. Yan, *Electrochem. Commun.*, 2014, **38**, 44–46.

(25) V. Lockett, R. Sedev, J. Ralston, M. Horne, and T. Rodopoulos, *J. Phys. Chem. C*, 2008, **112**, 7486–7495.

(26) M. Gnahm, T. Pajkossy, and D. M. Kolb, *Electrochim. Acta*, 2010, **55**, 6212–6217.

(27) M. Drüschler, B. Huber, and B. Roling, *J. Phys. Chem. C*, 2011, **115**, 6802–6808.

(28) T. Pajkossy and D. M. Kolb, *Electrochem. Commun.*, 2011, **13**, 284–286.

(29) B. Roling, M. Drüschler, and B. Huber, *Faraday Discuss.*, 2012, **154**, 303–311.

(30) Y. Su, J. Yan, M. Li, M. Zhang, and B. Mao, *J. Phys. Chem. C*, 2013, **117**, 205–212.

(31) L. Siinor, R. Arendi, K. Lust, and E. Lust, *J. Electroanal. Chem.*, 2013, **689**, 51–56.

(32) J. Wallauer, M. Drüschler, B. Huber, and B. Roling, *Z. Naturforsch. B*, 2013, **68**, 1143–1153.

(33) T. R. Gore, T. Bond, W. Zhang, R. W. J. Scott, and I. J. Burgess, *Electrochem. Commun.*, 2010, **12**, 1340–1343.

(34) M. Drüschler, B. Huber, S. Passerini, and B. Roling, *J. Phys. Chem. C*, 2010, **114**, 3614–3617.

(35) M. T. Alam, J. Masud, M. M. Islam, T. Okajima, and T. Ohsaka, *J. Phys. Chem. C*, 2011, **115**, 19797–19804.

(36) M. Mezger, H. Schröder, H. Reichert, S. Schramm, J. S. Okasinski, S. Schöder, V. Honkimäki, M. Deutsch, B. M. Ocko, J. Ralston, M. Rohwerder, M. Stratmann, and H. Dosch, *Science*, 2008, **322**, 424–428.

(37) R. Atkin, S. Z. El Abedin, R. Hayes, L. H. S. Gasparotto, N. Borisenko, and F. Endres, *J. Phys. Chem. C*, 2009, **113**, 13266–13272.

(38) N. Nishi, Y. Yasui, T. Uruga, H. Tanida, T. Yamada, S. Nakayama, H. Matsuoka, and T. Kakiuchi, *J. Chem. Phys.*, 2010, **132**, 164705(1–6).

(39) N. Nishi, T. Uruga, H. Tanida, and T. Kakiuchi, *Langmuir*, 2011, **27**, 7531–7536.

(40) N. Nishi, K. Kasuya, and T. Kakiuchi, *J. Phys. Chem. C*, 2012, **116**, 5097–5102.

(41) J. M. Black, M. B. Okatan, G. Feng, P. T. Cummings, S. V. Kalinin, and N. Balke, *Nano Energy*, 2015, **15**, 737–745.

(42) N. Nishi, T. Uruga, and H. Tanida, *J. Electroanal. Chem.*, 2015, **759**, 129–136.

(43) Y. Yasui, Y. Kitazumi, R. Ishimatsu, N. Nishi, and T. Kakiuchi, *J. Phys. Chem. B*, 2009, **113**, 3273–3276.

(44) I. Bou-Malham and L. Bureau, *Soft Matter*, 2010, **6**, 4062–4065.

(45) S. Makino, Y. Kitazumi, N. Nishi, and T. Kakiuchi, *Electrochem. Commun.*, 2011, **13**, 1365–1368.

(46) M. Drüschler, N. Borisenko, J. Wallauer, C. Winter, B. Huber, F. Endres, and B. Roling, *Phys. Chem. Chem. Phys.*, 2012, **14**, 5090–5099.

(47) N. Nishi, Y. Hirano, T. Motokawa, and T. Kakiuchi, *Phys. Chem. Chem. Phys.*, 2013, **15**, 11615–11619.

(48) A. Uysal, H. Zhou, G. Feng, S. S. Lee, S. Li, P. Fenter, P. T. Cummings, P. F. Fulvio, S. Dai, J. K. McDonough, and Y. Gogotsi, *J. Phys. Chem. C*, 2014, **118**, 569–574.

(49) A. Uysal, H. Zhou, G. Feng, S. S. Lee, S. Li, P. T. Cummings, P. F. Fulvio, S. Dai, J. K. McDonough, Y. Gogotsi, and P. Fenter, *J. Phys.-Condes. Matter*, 2015, **27**, 032101(1–9).

(50) T. Jaensch, J. Wallauer, and B. Roling, *J. Phys. Chem. C*, 2015, **119**, 4620–4626.

(51) N. Nishi, A. Hashimoto, E. Minami, and T. Sakka, *Phys. Chem. Chem. Phys.*, 2015, **17**, 5219–5226.

(52) M. M. Islam, M. T. Alam, T. Okajima, and T. Ohsaka, *J. Phys. Chem. B*, 2007, **111**, 12849–12856.

(53) F. Silva, C. Gomes, M. Figueiredo, R. Costa, A. Martins, and C. M. Pereira, *J. Electroanal. Chem.*, 2008, **622**, 153–160.

(54) M. T. Alam, M. M. Islam, T. Okajima, and T. Ohsaka, *J. Phys. Chem. C*, 2009, **113**, 6596–6601.

(55) R. Costa, C. M. Pereira, and F. Silva, *Phys. Chem. Chem. Phys.*, 2010, **12**, 11125–11132.

(56) M. Ammam, D. Di Caprio, and L. Gaillon, *Electrochim. Acta*, 2012, **61**, 207–215.

(57) R. Costa, C. M. Pereira, and F. Silva, *RSC Adv.*, 2013, **3**, 11697–11706.

(58) A. Lewandowski, T. Majkowski, and M. Galiński, *Z. Naturfors.*, 2009, **64a**, 263–268.

(59) Y. Han, S. Huang, and T. Yan, *J. Phys.-Condes. Matter*, 2014, **26**, 284103(1–10).

(60) R. Costa, C. M. Pereira, and A. Fernando Silva, *Electrochem. Commun.*, 2015, **57**, 10–13.

(61) A. Elbourne, S. McDonald, K. Voichovsky, F. Endres, G. G. Warr, and R. Atkin, *ACS Nano*, 2015, **9**, 7608–7620.

(62) G. Feng and P. T. Cummings, *J. Phys. Chem. Lett.*, 2011, **2**, 2859–2864.

(63) G. Feng, D.-e. Jiang, and P. T. Cummings, *J. Chem. Theory Comput.*, 2012, **8**, 1058–1063.

(64) J. Vatamanu, O. Borodin, D. Bedrov, and G. D. Smith, *J. Phys. Chem. C*, 2012, **116**, 7940–7951.

(65) Z. Hu, J. Vatamanu, O. Borodin, and D. Bedrov, *Electrochim. Acta*, 2014, **145**, 40–52.

(66) G. Feng, S. Li, W. Zhao, and P. T. Cummings, *AICHE J.*, 2015, **61**, 3022–3028.

(67) M. J. Earle, C. M. Gordon, N. V. Plechkova, K. R. Seddon, and T. Welton, *Anal. Chem.*, 2007, **79**, 758–764.

(68) S. Dzyuba and R. Bartsch, *ChemPhysChem*, 2002, **3**, 161–166.

(69) A. Wandschneider, J. K. Lehmann, and A. Heintz, *J. Chem. Eng. Data*, 2008, **53**, 596–599.

(70) D. Ambrose, *Metrologia*, 1990, **27**, 245–247.

(71) M. Tariq, M. G. Freire, B. Saramago, J. A. P. Coutinho, J. N. Canongia Lopes, and L. P. N. Rebelo, *Chem. Soc. Rev.*, 2012, **41**, 829–868.

(72) K. Yajima, H. Moriyama, and J. Oishi, *J. Phys. Chem.*, 1984, **88**, 4390–4394.

(73) H. Helmholtz, *Ann. Phys. Chem.*, 1853, **165**, 211–233.

(74) H. Weingaertner, *Z. Phys. Chem.*, 2006, **220**, 1395–1405.

(75) J. Lopes and A. Padua, *J. Phys. Chem. B*, 2004, **108**, 16893–16898.

(76) J. Vatamanu, O. Borodin, and G. D. Smith, *J. Am. Chem. Soc.*, 2010, **132**, 14825–14833.

(77) D.-e. Jiang, D. Meng, and J. Wu, *Chem. Phys. Lett.*, 2011, **504**, 153–158.

(78) S. Lamperski, J. Sosnowska, L. B. Bhuiyan, and D. Henderson, *J. Chem. Phys.*, 2014, **140**, 014704(1–4).

(79) A. C. Maggs and R. Podgornik, *Soft Matter*, 2016, **12**, 1219–1229.

(80) M. V. Fedorov and A. A. Kornyshev, *J. Phys. Chem. B*, 2008, **112**, 11868–11872.

(81) M. Kaja, W. Silvestre-Alcantara, S. Lamperski, D. Henderson, and L. B. Bhuiyan, *Mol. Phys.*, 2015, **113**, 1043–1052.

(82) V. Ivaništšev, K. Kirchner, T. Kirchner, and M. V. Fedorov, *J. Phys.-Condes. Matter*, 2015, **27**, 102101(1–5).

(83) D. C. Grahame, *Chem. Rev.*, 1947, **41**, 441–501.

(84) N. Nishi, J. Uchiyashiki, R. Oogami, and T. Sakka, *Thin Solid Films*, 2014, **571**, 735–738.

(85) K. Motobayashi, K. Minami, N. Nishi, T. Sakka, and M. Osawa, *J. Phys. Chem. Lett.*, 2013, **4**, 3110–3114.

(86) M. Z. Bazant, B. D. Storey, and A. A. Kornyshev, *Phys. Rev. Lett.*, 2011, **106**, 046102(1–4).

(87) G. Feng, J. Huang, B. G. Sumpter, V. Meunier, and R. Qiao, *Phys. Chem. Chem. Phys.*, 2011, **13**, 14723–14734.

(88) H. Zhao, *Phys. Rev. E*, 2011, **84**, 051504(1–10).

(89) V. Demery, D. S. Dean, T. C. Hammant, R. R. Horgan, and R. Podgornik, *EPL*, 2012, **97**, 28004(1–5).

(90) A. Yochelis, M. B. Singh, and I. Visoly-Fisher, *Chem. Mat.*, 2015, **27**, 4169–4179.

(91) Z. A. Goodwin, G. Feng, and A. A. Kornyshev, *Electrochim. Acta*, 2017, **225**, 190–197.

(92) S. Rivera-Rubero and S. Baldelli, *J. Phys. Chem. B*, 2004, **108**, 15133–15140.

(93) N. Nanbu, T. Kato, Y. Sasaki, and F. Kitamura, *Electrochemistry*, 2005, **73**, 610–613.

(94) C. Pinilla, M. Del Popolo, R. Lynden-Bell, and J. Kohanoff, *J. Phys. Chem. B*, 2005, **109**, 17922–17927.

(95) S. A. Kislenko, I. S. Samoylov, and R. H. Amirov, *Phys. Chem. Chem. Phys.*, 2009, **11**, 5584–5590.

(96) S. Wang, S. Li, Z. Cao, and T. Yan, *J. Phys. Chem. C*, 2010, **114**, 990–995.

(97) X. Si, S. Li, Y. Wang, S. Ye, and T. Yan, *ChemPhysChem*, 2012, **13**, 1671–1676.

(98) D. Dimitrov, N. Raev, and K. Semerdzhiev, *Phys. Chem. Chem. Phys.*, 2001, **3**, 448–452.

Figure captions

Fig. 1 Electrocapillarity at the $[C_2mim^+][TFSA^-]$|Hg interface (red solid circles) and at the $[C_2mim^+]BF_4^-$|Hg interface (blue solid squares)[51] measured by pendant drop method with error bars of one standard deviation.

Fig. 2 Surface charge density on Hg (q_M) as a function of the electrode potential at the $[C_2mim^+][TFSA^-]$|Hg interface (red solid circles) and at the $[C_2mim^+]BF_4^-$|Hg interface (blue solid squares)[51] with error bars of one standard deviation. Inset is a magnified one around $q_M = 0$ for the $[C_2mim^+][TFSA^-]$|Hg interface. The solid curve in the inset is from quadratic least squares regression with weights for four consecutive data points around $q_M = 0$, which evaluated E_{pzc} to be -0.373 ± 0.002 V.

Fig. 3 Zero-frequency differential capacitance as a function of the electrode potential (a) at the $[C_2mim^+][TFSA^-]$|Hg interface (red solid circles) and (b) at the $[C_2mim^+]BF_4^-$|Hg interface (blue solid squares)[51] with error bars of one standard deviation. Vertical dotted lines are at the potential of zero charge. The open circles and squares are differential capacitance at 100 Hz measured using EIS. The dashed lines are a fitted curve of Eq.2 to experimental plots within the potential region (a) from -0.7 to -0.2 V and (b) from -0.55 to -0.15 V.

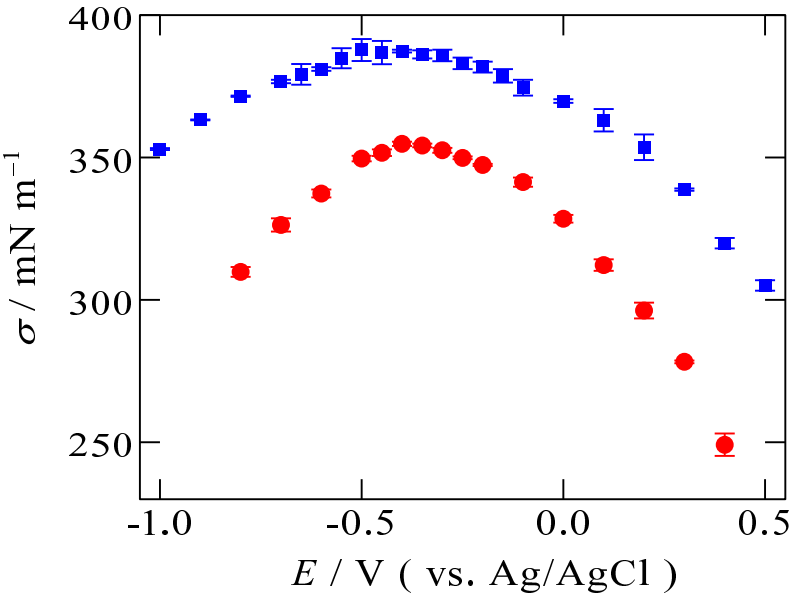

Fig.1 (Nishi et al.)

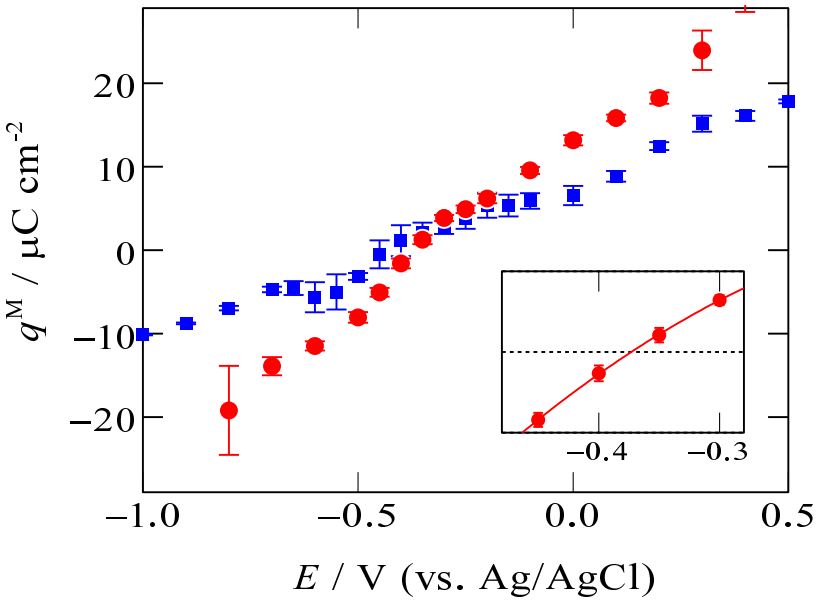

Fig.2 (Nishi et al.)

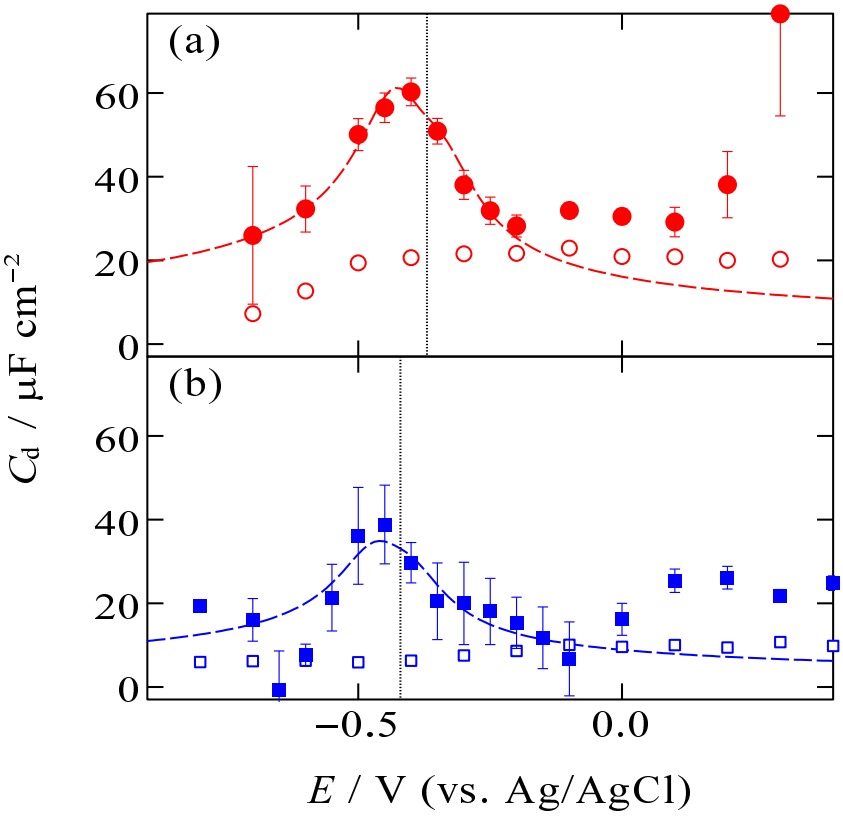

Fig.3 (Nishi et al.)